IMAGE-VARIANT INTERIOR ORIENTATION AND SENSOR MODELLING OF HIGH-QUALITY DIGITAL CAMERAS

H. Hastedt*, Th. Luhmann, W. Tecklenburg

Institute for Applied Photogrammetry and Geoinformatics, University of Applied Sciences Oldenburg,
Ofener Straße 16/19, D-26121 Oldenburg, Germany – iapg@fh-oldenburg.de/*h.hastedt@vermes.fh-oldenburg.de

Commission V, WG V/1

KEY WORDS: camera calibration, image-variant interior orientation, finite elements, distortion, accuracy, bundle adjustment, guideline VDI/VDE 2634

ABSTRACT:

Nowadays digital high-resolution consumer cameras are increasingly used in close-range photogrammetry. These partial-metric cameras do not meet photogrammetric requirements as (conventional) metric cameras do. Especially the mechanical construction of these cameras is instable. Therefore extended mathematical models for camera calibration are required to model all instabilities and influences sufficiently. An approach including image-variant interior orientation for camera modelling is discussed. A correction model with finite elements is added to the mathematical model that provides the correction of remaining errors in sensor space. All parameters are estimated simultaneously in a bundle adjustment. Based on the German guideline VDI/VDE 2634 for acceptance and reverification test of optical 3D measuring systems the discussed camera modelling is tested by different camera lens combinations and configurations of imaging. The results express the importance of the camera model and the investigations concerning verification tests as described in this paper. Significant improvements of accuracy have been achieved with respect to conventional calibration techniques within self-calibration bundle adjustment.

1. INTRODUCTION

High quality digital cameras are increasingly used for industrial metrology and machine vision applications. Most of these cameras are designed for photo-journalism purposes and do not meet photogrammetric requirements as conventional metric-cameras do (Shortis et al. 1998; Luhmann & Wendt 2000). In particular these partial-metric cameras show high instability concerning the fixed CCD-array with respect to the lens. The system's accuracy mainly depends on image resolution, image scale, image measurement precision and network design (Fraser et al. 1998). Relative precision of 1:50000 up to 1:80000 is required for most industrial applications. Internal accuracy up to 1:100000 can be achieved using a Kodak DCS 460 (Shortis et al. 1998). Image measurement precision of 0.02 – 0.05 Pixel, respectively 0.25µm in image space can be achieved, hence it is fundamental for the accuracy of the photogrammetric bundle adjustment.

The calibration of still-video cameras like the Kodak DCS 460 or the Fuji S1 Pro is necessary to consider and eliminate systematic errors (Shortis et al. 1998). Conventional mathematical models for camera calibration assume a stable interior orientation for one set of images over the whole period of image acquisition. Principal distance (c_k), principal point (x_h,y_h), radial-symmetric lens distortion (a_1,a_2,a_3), decentring of lenses by tangential and asymmetric distortion (b_1,b_2) and global sensor properties such as affinity and sheering (c_1,c_2) are estimated within self-calibrating systems.

Different investigations have been made to take deformations of film and sensor plane into account (e.g. CAP). Munji (1986) reports on the application of finite elements for the determination of local imaging errors of partial-metric cameras. The behaviour of the principal point for Kodak cameras with assumed fix principal distance based on several sets of images is exposed at Shortis et al. (1998). Fraser et al. (1992) and Dold (1997) report on the influence of variation of distortion within the photographic field and gained improvement in accuracy for special applications.

It can not be assumed that camera parameters remain stable over the whole period of image acquisition. Gravity takes effect with different viewing directions. Long periods of image acquisition yield to heat the camera with increasing influences on the photogrammetric system (Jantos et al. 2002). The camera is subject to intense mechanical influences by the user; especially hand-held shots are influenced by the users handling and can yield to varying strains of the camera body (Tecklenburg et al. 2000).

These effects are investigated by the discussed extended model for camera calibration. An image-variant interior orientation is added to the camera model which describes variation in principal distance and principal point. As a major result the possible displacement and rotation of the lens with respect to the image sensor are compensated by this model, similar to the approach of Maas (1998). In order to compensate sensor based influences (especially sensor unflatness) as well as all remaining lens effects not considered within radial-symmetric lens distortion, a finite-elements correction grid has been chosen. This raster-wise correction grid based on anchor points is distributed according to an a priori grid width.

This approach is verified by various sets of images of a testfield based on the German guideline VDI/VDE 2634. Different photogrammetric projects are accessable of an own control field with reference points for comparability and quality of the camera and its parameters. Mainly two cameras (Kodak DCS 460 and Fuji S1 Pro) are tested by different sets of images of the described testfield. The results are presented and discussed.

2. MATHEMATICAL MODEL

2.1 Image-variant parameters

Usually camera parameters are applied identically for all images of a photogrammetric project. Distortion parameters are defined with respect to the principal point. Then the standard observation equation (1) yield

$$x' = x'_0 - c \cdot \frac{r_{11} \cdot (X_p - X_0) + r_{21} \cdot (Y_p - Y_0) + r_{31} \cdot (Z_p - Z_0)}{r_{13} \cdot (X_p - X_0) + r_{23} \cdot (Y_p - Y_0) + r_{33} \cdot (Z_p - Z_0)} + dx'$$
$$y' = y'_0 - c \cdot \frac{r_{12} \cdot (X_p - X_0) + r_{22} \cdot (Y_p - Y_0) + r_{32} \cdot (Z_p - Z_0)}{r_{13} \cdot (X_p - X_0) + r_{23} \cdot (Y_p - Y_0) + r_{33} \cdot (Z_p - Z_0)} + dy' \quad (1)$$

The expected variations of principal distance and principal point are estimated in the range of a few hundreds of a millimetre. Therefore these parameters are introduced as observed unknowns to the bundle adjustment weighted according to the a priori accuracy chosen by the user. Using this proceeding the bundle adjustment results do not become "weak" and smearing effects caused by correlation between other parameters can be avoided.

2.2 Finite elements correction grid

In order to consider the remaining effects – non-variant effects – a finite-element correction grid based on anchor points is implemented (Fig. 1). In this case the non-variant effects are given by all lens and sensor-based influences that are not considered by radial-symmetric distortion parameters. In addition this correction grid covers possible sensor unflatness and influences which are usually not taken into account by conventional calibration models.

Figure 1: Principle of the correction grid applied for a digital camera (Kodak DCS)

Each grid point provides corresponding corrections as plane vectors. The correction values for a measured image point are interpolated according to a linear equation (3; Fig. 2).

Camera modelling with image-variant parameters causes three more parameters per image to be estimated within the bundle adjustment. Hence the number of unknown grows up to nine per image. These parameters describe the variation of the principal distance and the shift of the principal point, hence the possible displacement and rotation of the lens with respect to the image sensor are compensated by this approach using extended standard observation equation (2).

The variation of the principal point affects the lens distortion with respect to the image plane. Consequently this can no longer be modelled as a function of image coordinates rather than a function of imaging angle. Additionally, the local shift of principal point influences the real effect of distortion for each image position.

$$x' = (x'_0 + \Delta x'_i) - (c + \Delta c_i) \cdot \frac{r_{11} \cdot (X_p - X_0) + r_{21} \cdot (Y_p - Y_0) + r_{31} \cdot (Z_p - Z_0)}{r_{13} \cdot (X_p - X_0) + r_{23} \cdot (Y_p - Y_0) + r_{33} \cdot (Z_p - Z_0)} + dx'_{\langle \ldots \Delta c_i, \Delta x'_i, \Delta y'_i \rangle}$$
$$y' = (y'_0 + \Delta y'_i) - (c + \Delta c_i) \cdot \frac{r_{12} \cdot (X_p - X_0) + r_{22} \cdot (Y_p - Y_0) + r_{32} \cdot (Z_p - Z_0)}{r_{13} \cdot (X_p - X_0) + r_{23} \cdot (Y_p - Y_0) + r_{33} \cdot (Z_p - Z_0)} + dy'_{\langle \ldots \Delta c_i, \Delta x'_i, \Delta y'_i \rangle} \quad (2)$$
$$i = 1, \text{number of images}$$

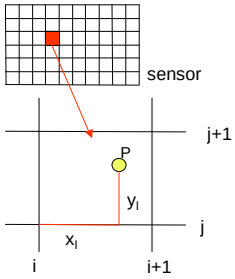

Figure 2: Interpolation within the correction grid

$$\begin{aligned} x_{korr} = {} & (1 - x_l - y_l + x_l \cdot y_l) \cdot k_{x[i,j]} \\ & + (x_l - x_l \cdot y_l) \cdot k_{x[i+1,j]} \\ & + (y_l - x_l \cdot y_l) \cdot k_{x[i,j+1]} \\ & + x_l \cdot y_l \cdot k_{x[i+1,j+1]} \end{aligned} \quad (3)$$

Here x_{korr} denotes the correction of the measured image coordinate (x), the coordinates x_l,y_l describe the local position of the measured image point inside the grid element and the elements $k_x[i,j]$, $k_x[i+1,j]$, $k_x[i,j+1]$, $k_x[i+1,j+1]$ identify the participating grid points. In analogy the similar equation results for the image coordinate (y). The collinearity equations are extended by the terms described above.

Separating random measuring errors from real sensor deformations and not modelled imaging errors of the lens, curvature constraints (4) are added as pseudo observations (Kraus 2000).

$$0 = (k_{x[i,j-1]} - k_{x[i,j]}) - (k_{x[i,j]} - k_{x[i,j+1]})$$
$$0 = (k_{x[i-1,j]} - k_{x[i,j]}) - (k_{x[i,j]} - k_{x[i+1,j]}) \quad (4)$$
(similar function for $k_{y[]]}$)

These equations are applied inside the correction grid in horizontal and vertical direction. This leads to a new group of observations within the equation system. The equations are introduced with an appropriate accuracy (globally estimated a priori weight) depending on the estimated unflatness (roughness) of the correction grid and the actual number of

image measurements for one grid element of one set of images. Additionally, these constraints avoid possible singularities of the adjustment as they might occur for grid elements without measured image position.

3. INVESTIGATIONS AND RESULTS

The exposed extended mathematical model for camera calibration ought to be tested and determined by different data sets. The German guideline for acceptance and reverification test of optical 3D measuring systems proposes to have a testfield with a range of 2m x 2m x 1.5m (VDI 2001). The maximum permissible error of length measurement needs to be tested by at least seven different measuring lines distributed in a specific manner (Luhmann & Wendt 2000a). The quality of the photogrammetric system is reflected by the error of length measurement with respect to the expected accuracy.

For evaluation and comparing purposes a 3-D testfield (Fig. 3) with a dimension of app. 2m x 2m x 2m (exterior testfield) has been designed for camera calibration. This test range covers app. 200 object points. In the centre a second 3-D testfield of app. 0.8m x 0.8m x 0.8m is placed forming the reference testfield. The reference field consists of 16 reference points (Fig. 3) whereof 120 different distances are computable. The reference points are measured by a coordinate measuring machine (CMM) by two independent measuring passes. An absolute deviation of the reference coordinates between the two passes of one CMM results with maximal 15µm. The eccentricities of the retro-reflective targets to the CMM measured target axis have been verified. The values do not effect the photogrammetric adjustment. The systems scale is based on one scale bar in y-direction. The scale bar has a verified standard deviation a priori of 5µm.

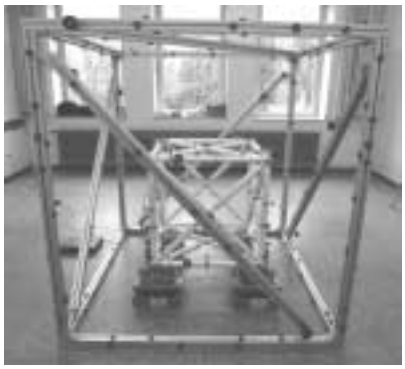

testfield based on guideline VDI/VDE 2634 with interior reference testfield

reference testfield

principle of reference points (Hubbs-targets)

Figure 3: Testfields and reference points

Four data sets of different configurations, varying camera handling and camera-lens-combinations (CLC) (Table 1) are taken as hand-held shots. With an Fuji S1 Pro and a 28mm lens two sets of images (CLC1,2) are taken whereby as few as possible imaging directions (Table 2) are mixed among one other. Therefore the different camera stations are visited several times for taking images. These sets of images are taken by careful camera handling. In contrast a data set with a Kodak DCS 460 (not stabilised CCD-sensor) and the same 28mm lens (CLC3) was taken. All necessary images in all imaging directions are taken at once by careless handling. For comparing aspects the calibration results of the DCS Pro Back 645M are added to the analysis (Table 1).

CLC	camera	lens	σ [µm]	$RMS_{(XYZ)}$ Eq. (5)	Relative precision	
1	Fuji S1 Pro	28 mm (1)	0.406	0.0543	1:49000	#
2	Fuji S1 Pro	28 mm (1)	0.346	0.0389	1:69000	#
3	DCS 460	28 mm (1)	0.352	0.0491	1:55000	*
4	DCS Pro Back 645M	35 mm	0.333	0.0337	1:80000	-

Table 1: Data set overview and adjustment results

\# rolling in four directions, care handling, 5mm targets
* rolling in four directions, careless handling, 5mm targets
\- all investigations on this are legible at Jantos (2002)

0°	-90°	+90°	180°
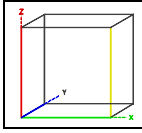	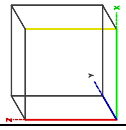	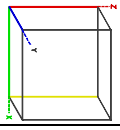	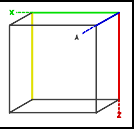

Table 2: Principle of imaging direction

Exposures are taken in four imaging directions with a proportion of 40:12:12:16 for the directions plotted in Table 2. The camera stations are chosen around the 3-D testfield with 0.5 to 2m object distance in 3 main height levels (bottom – mid level – above the testfield).

All image points are measured by ellipse fitting. The accuracy of the ellipse fitting method yield to 0.39µm for CLC1, 0.33µm for CLC2 and 0.44µm for CLC3 a priori. The average of ellipse sizes for all data sets results in less than 6 pixel.

3.1 Interior accuracy

The image measurement precision a posteriori lies between 0.3 and 0.4µm. The object point accuracy, in this case RMS values, for X, Y and Z direction for all object points within the photogrammetric projects (CLC1-3) yields a mean value of 30µm. An average of 20µm could be obtained with the DCS Pro Back 645M (CLC4). This leads to an object precision $RMS_{(XYZ)}$ (5) of 54µm up to 34µm, the corresponding relative precision results in 1:49000 – 1:80000 (Table 1).

$$RMS_{(XYZ)} = \sqrt{[RMS(X)]^2 + [RMS(Y)]^2 + [RMS(Z)]^2} \qquad (5)$$

The required relative precision for standard industrial applications is obtained with these data sets, though they are borderline cases because of image configuration with almost exclusively sensor fulfilling exposures and a mean value for target size of less than 6 pixel. The reference points and scale points (Hubbs-targets) have a size of 6.35mm. The RMS values

for the reference points are much better as they are in the centre of the system. A problem constitutes the adjustment of the reference points in two horizontal levels. Hence, this yields to almost sloped and small ellipses. However, there was no better alternative in view of getting the reference coordinates measured with an independent measuring system with an appropriate accuracy.

3.2 Image-variant interior orientation and correction grid

Due to high variation in image-variant parameters, particularly in y-direction, and especially for the CLC3 caused by careless handling, high peaks in positive and negative direction could be expected. This is figured in the adjustment results. Fig. 4 illustrates the variation of image-variant interior parameters in chronological order of exposures (exemplary for CLC1).

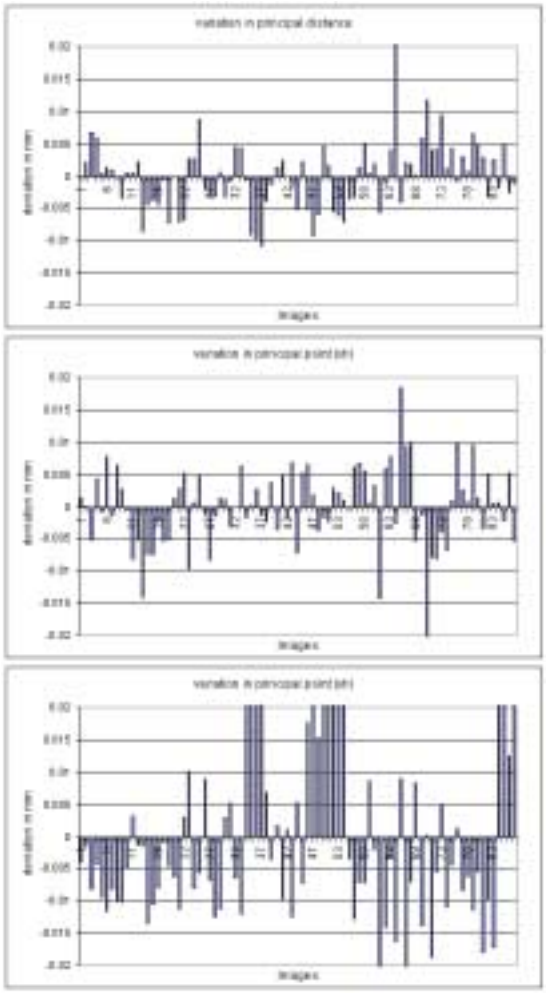

Figure 4: Variation in principal distance and principal point

The behaviour of both cameras, the Fuji S1 Pro and the Kodak DCS 460, is similar. By rolling the camera around the optical axis with –90° negative deviations occur in x-direction while they are positive in y-direction. Rolling through +90° yields negative values for y-direction and reverse positive in x-direction. High positive deviations in y-direction arise from rolling through 180°.

Shortis et al. (1998) assumed that the position of the principal point varies in a specific manner with respect to the imaging direction. Likewise shown in Fig. 5b for the CLC2 the position varies around a coordinate-origin in different directions. This assumption does not occur for each data set as it is dependent on the stability and sensitivity of the used camera.

The principal point mainly varies like assumed. Different spread effects are visible while the main variation of the position of one viewing direction is similar and varies in an average of ±20µm.

a

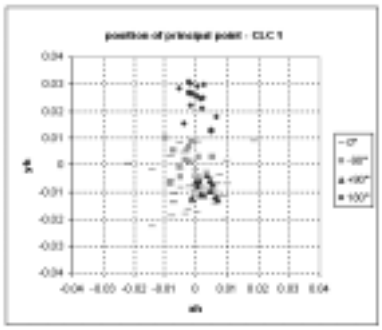

b

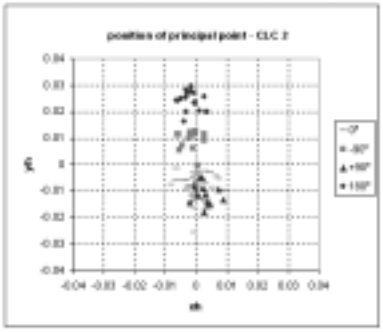

c

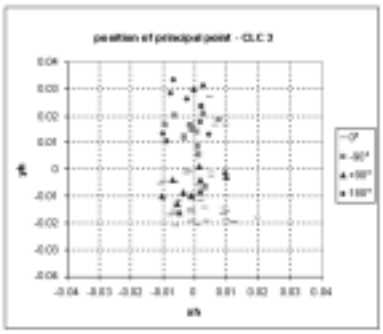

Figure 5: location-plot of image-variant principal point

The values of principal distance and principal point of each image of one data set varies within ±33µm where the maximum and minimum values are separately listed in Table 3.

	CLC1	CLC2	CLC3
Mean values			
c_k	29.15337	29.15015	28.65453
x_h	0.29152	0.26663	0.55286
y_h	-0.05304	-0.11359	0.23434
Maximum Minimum			
c_k	0.02522 -0.01070	0.01034 -0.01677	0.00999 -0.01288
x_h	0.01853 -0.02181	0.00896 -0.00827	0.0198 -0.01063
y_h	0.03072 -0.02276	0.02961 -0.02563	0.03329 -0.02115

Table 3: Values of image-variant parameters

The principal distance mainly varies within ±10µm for all sets of images. Having a closer look at the behaviour of the principal

point some differences are coming up. While the principal point in x-directions varies within ±10µm as the principal distance does equally, the variation in y-direction is higher than expected. The deviations range within ±20µm with much more peaks up to ±30µm. The image-variant principal point for CLC3 varies more compared to the other sets of images.

As it is shown in Fig. 6 for the Fuji S1 Pro the correction grid covers the fact of having non-squared pixels using a resolution of 2304 by 1536 pixel. The correction grid is based on a grid width of 2mm. The pattern of points represents the image measurements with respect to the sensor. The plot shows the reproducibility of the correction grid of one camera. The marginally difference results from slight variation of image point spread. The correction values concerning the DCS 460 indicate no significant deformations.

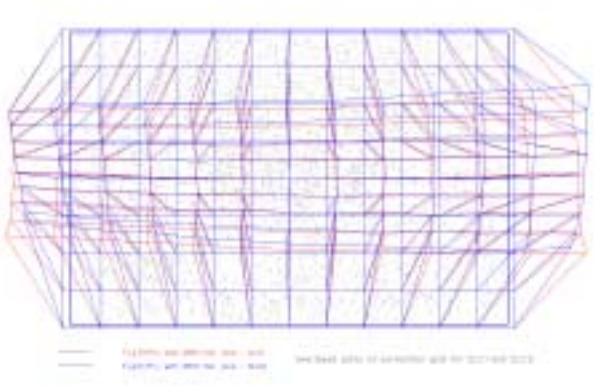

Figure 6: Correction grid for CLC1 and CLC2 – 100x inflated

3.3 Exterior accuracy

For the evaluation of the photogrammetric adjustment the exterior accuracy related to reference distances is finally to be estimated. In this case 120 distances, derived from 16 reference points, are computable. The reference coordinates are only measured once and underlie high variation of temperature and transport influences from the CMM to the photogrammetric laboratory. To evaluate the influences by temperature, constant measurements of temperature are performed during and before image acquisition. The results of the photogrammetric system are corrected with respect to the co-efficient of expansion. The system scale is based on one scale in y-direction. The scale has an a priori accuracy of 5µm (calibrated by PTB).
For CLC1-3 Fig. 7 shows the resulting errors of length measurement (LME). CLC1 and CLC2 are trend-corrected with 30µm/m, CLC3 is trend-corrected with 40µm/m. Obviously a length-dependent part for the adjustment result is remaining. Beneath this general trend a continuity concerning the length measuring error (LME) with respect to the discrete reference points is visible. All LME for distances with point 209 remain negative and form minimum in LME. Some other effects by reference points are remaining equally for all data sets.

Having a view on the collectivity of LME for each data set an absolute mean of LME (6) and a RMS value for LME (7) can be determined.

$$LME_{abs} = \frac{\sum l_{abs}}{n} \tag{6}$$

$$RMS_{LME} = \sqrt{\frac{\sum l^2}{n}} \tag{7}$$

Table 4 shows the maximal corrected deviation in positive and negative direction and mean values of LME.

	Max. deviation		LME_{abs}	RMS_{LME}
CLC 1	+0.0629	-0.0530	0.0170	0.0217
CLC 2	+0.0450	-0.0410	0.0129	0.0160
CLC 3	+0.0683	-0.0960	0.0346	0.0423

Table 4: Analysis of length measuring error

For further analysis the 1σ, 2σ and 3σ standard deviation for one distance computed of 2 object points (8) are calculated for the additional observation that implies the system scale (Table 5, the %-value points the LME within the Sigma value).

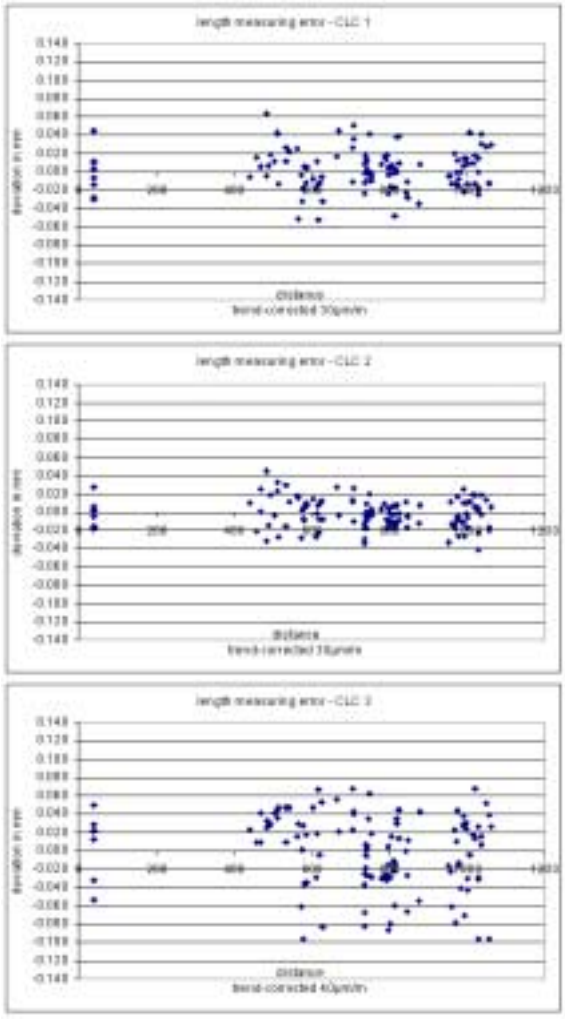

Figure 7: Diagram of length measuring error

$$s_s^2 = \left(\frac{\partial s}{\partial x_1}\right)^2 * s_{x_1}^2 + \left(\frac{\partial s}{\partial x_2}\right)^2 * s_{x_2}^2 + \left(\frac{\partial s}{\partial y_1}\right)^2 * s_{y_2}^2 + \left(\frac{\partial s}{\partial y_2}\right)^2 * s_{y_2}^2 + \left(\frac{\partial s}{\partial z_1}\right)^2 * s_{z_1}^2 + \left(\frac{\partial s}{\partial z_2}\right)^2 * s_{z_2}^2 \tag{8}$$

These values are taken as expected deviation for LME. 67 – 97% of all LME are captured within 2σ, respectively ±40µm in object space. The CLC3 taken with the Kodak DCS 460 shows high spread in LME. This probably results from the careless handling and the fact of using an instable camera, in this case the CCD-array is only fixed with one screw.

	1σ		2σ		3σ	
	value	%	value	%	value	%
CLC 1	0.0182	67	0.0364	88	0.0547	99
CLC 2	0.0167	70	0.0335	97	0.0503	100
CLC 3	0.0198	28	0.0397	67	0.0595	84

Table 5: Percentage of LME within expected deviation

The extended model for camera calibration achieves significant improvements of accuracy as finally pointed out by results of the same data sets with conventional bundle-invariant camera model (Table 6). An improvement up to 25µm in object space could be achieved including image-variant parameters.

	σ [µm]	$RMS_{(XYZ)}$	Relative precision
CLC1	0.553	0.0655	1:41000
CLC2	0.506	0.0611	1:44000
CLC3	0.609	0.0747	1:36000

Table 6: results by conventional camera model

4. CONCLUSIONS

Because of nowadays mostly used high-quality cameras – partial-metric cameras – new mathematical approaches are necessary to model all instabilities and camera based influences sufficiently. With the implementation of image-variant principal distance, image-variant principal point and an additional correction grid to model remaining sensor and lens based influences these instabilities can be considered. In general the adjustment results, especially the variation in image-variant parameters, are highly dependent on imaging direction. The variation in y-direction points peaks up to 33µm to the mean value. Using an invariant interior orientation the effects of image-variant part are smeared to other parameters. The smearing effects cause probably wrong results. Data sets with high instable interior orientation might not be computable by conventional approaches. The mentioned data set of the DCS Pro Back 645M proofs this assumption. The CCD-array is mounted to the camera body and relocatable in x-direction. An offset of about 100µm during image acquisition with the DCS 645M was only computable with the described image-variant mathematical model. Significant improvements in accuracy with respect to a modelling with bundle-invariant interior orientation have been achieved.

The presented bundles do not figure optimal configuration because of almost exclusively fulfilling images and influences by the image measurements of the object point with small ellipses caused by point diameter of only 5mm in object space. Improvements of image acquisition configuration need to be required. The 3-D testfield for verification of the bundle results needs closer research. At least one additional measurement of the reference points is necessary to eliminate the remaining length-dependent part in the length measurement errors. The overbalancing part of LME in the range of ±40µm under consideration of instable parts and with careful handling of the camera point high-accuracy 3-D results.

5. FURTHER INVESTIGATIONS

For further project work a major research will be addressed to the improvement of imaging acquisition configuration. The optimal number of images and images per imaging direction, camera stations by optimal efficiency need to be verified. This investigation depends on the 3-D testfield, the reference coordinates and the knowledge of the testfield's behaviour with respect to different exterior influences.

Beyond analyses concerning accuracy of three-dimensional objects and verification based on the German guideline VDI/VDE 2634 will be done.

6. REFERENCES

Dold, J. (1997): Ein hybrides photogrammetrisches Industriemeßsystem höchster Genauigkeit und seine Überprüfung; Schriftenreihe Universität der Bundeswehr München, Heft 54.

Fraser, C.S., Shortis, M.R. (1992): Variation of Distortion within the Photographic Field; PE&RS, Vol. 58, No. 6, June 1992, pp. 851-855.

Jantos, R., Luhmann, Th., Peipe, J., Schneider, C.-T. (2002): Photogrammetric Performance Evaluation of the Kodak DCS Pro Back; ISPRS Symposium Commission V, Corfu 2002.

Kraus, K. (2000): Photogrammetrie, Band 3, Topographische Informationssysteme; Dümmler Verlag, Bonn, p. 188ff.

Luhmann, Th. (2000): Nahbereichsphotogrammetrie; Wichmann Verlag, Heidelberg.

Luhmann, Th., Wendt, K. (2000): Recommendations for an acceptance and verification test of optical 3D measurement systems; International Archives for Photogrammetry and Remote Sensing, Vol. 33/5, pp. 493-499; Amsterdam.

Maas, H.-G. (1998): Ein Ansatz zur Selbstkalibrierung von Kameras mit instabiler innerer Orientierung; Publikationen der DGPF, Band 7, München 1998.

Munji, R.A.H. (1986): Self-calibration using the finite element approach; Photogrammetric Engineering and Remote Sensing, Vol. 52, No. 3, March 1986, pp. 411-418.

Munji, R.A.H. (1986): Calibration of non-metric cameras using the finite element method; Photogrammetric Engineering and Remote Sensing, Vol. 52, No. 8, August 1986, pp. 1201-1205.

Shortis, M.R., Robson, S., Beyer, H.A.(1998): Principal point behaviour and calibration parameter models for Kodak DCS cameras; Photogrammetric Record, 16(92): 165-186

Tecklenburg, W.; Luhmann, Th.; Hastedt, H. (2000): Camera modelling with image-variant parameters and Finite Elements; Optical 3D; Vienna

VDI/VDE 2634 (2001): Optical 3-D measuring systems – Imaging systems with point-by-point probing. VDI, Düsseldorf.